Applied Physics Letters

RESEARCH ARTICLE | JULY 09 2025

Field- and frequency-tunable magnon–phonon resonances in arrays of ferromagnetic nanostripes

Special Collection: Strain-controlled Magnetism: From Fundamental Phenomena to Devices

P. Carrara ; M. Brioschi ; R. Silvani ; A. O. Adeyeye ; G. Panaccione ; G. Gubbiotti ; G. Rossi ; R. Cucini

Check for updates

Appl. Phys. Lett. 127, 012407 (2025)
https://doi.org/10.1063/5.0278334

View Online
Export Citation

Articles You May Be Interested In

Propagating and reflecting of spin wave in permalloy nanostrip with 360° domain wall

J. Appl. Phys. (January 2014)

Mechanism of reversing the Neel domain walls in the Co nanostripes with transverse magnetic anisotropy

Appl. Phys. Lett. (December 2012)

Electrical generation and propagation of spin waves in antiferromagnetic thin-film nanostrips

Appl. Phys. Lett. (June 2019)

22 July 2025 09:02:09

AIP Publishing

Applied Physics Letters ARTICLE pubs.aip.org/aip/apl

Field- and frequency-tunable magnon–phonon resonances in arrays of ferromagnetic nanostripes

Cite as: Appl. Phys. Lett. **127**, 012407 (2025); doi: 10.1063/5.0278334
Submitted: 29 April 2025 · Accepted: 20 June 2025 ·
Published Online: 9 July 2025

View Online Export Citation CrossMark

P. Carrara,[1,2,3] M. Brioschi,[2,3] R. Silvani,[4] A. O. Adeyeye,[5] G. Panaccione,[3] G. Gubbiotti,[6,a)] G. Rossi,[2,3,a)] and R. Cucini[3]

AFFILIATIONS

[1]Sorbonne Université, CNRS, Institut des NanoSciences de Paris INSP, 75005 Paris, France
[2]Dipartimento di Fisica, Università degli Studi di Milano, 20133 Milano, Italy
[3]CNR-Istituto Officina dei Materiali (IOM), Unità di Trieste, 34149 Basovizza (TS), Italy
[4]Dipartimento di Fisica e Geologia, Università di Perugia, 06123 Perugia, Italy
[5]Department of Physics, Durham University, Durham DH1 3LE, United Kingdom
[6]CNR-Istituto Officina dei Materiali (IOM), Unità di Perugia, 06123 Perugia, Italy

Note: This paper is part of the Special Topic, Strain-controlled Magnetism: From Fundamental Phenomena to Devices.
[a)]**Authors to whom correspondence should be addressed:** gubbiotti@iom.cnr.it and giorgio.rossi2@unimi.it

ABSTRACT

The coupling of lattice and magnetization dynamics is a topic of growing interest, with significant implications for novel solid-state technologies. In this work, we investigate arrays of ferromagnetic Fe/Permalloy nanostripes. A time-resolved optical approach enables the study of magnonic and phononic excitations, as well as their coupling at mode crossings. The field-dependent frequencies were also measured using Brillouin light scattering spectroscopy and corroborated by micromagnetic simulations for different in-plane directions of an external magnetic field. We find that the acoustic and magnonic excitations can be tuned in frequency and magnetic field by adjusting the array periodicity, filling ratio, as well as the orientation of the nanostripes relative to the external field. Additionally, we discuss the presence of features in the signal intensity at the magnon–phonon crossings, introduced by dynamical phase effects due to the impulsive coherent excitation.

© 2025 Author(s). All article content, except where otherwise noted, is licensed under a Creative Commons Attribution (CC BY) license (https://creativecommons.org/licenses/by/4.0/). https://doi.org/10.1063/5.0278334

22 July 2025 09:02:09

Magnonics, namely the application-oriented study of magnons, emerged as a relevant research direction in the quest for low-consumption fast technologies for next-generation electronics and information processing.[1,2] Magnons can propagate without Joule loss, potentially enabling high-rate and energy-efficient information transmission. Moreover, they naturally couple to spin-based memory and logic units, suggesting the design of all-spin-based platforms.[3] A limitation in this approach is the low excitation efficiency employing inductive electromagnetic sources and the short decay length. Both issues can be addressed by hybridizing magnons with other quasi-particles, an approach that gave birth to hybrid magnonics.[4] A relevant approach is the hybridization of magnons with acoustic phonons in magnetic thin films[5,6] and nanostructures,[7,8] leading to the formation of quasi-particles known as magnon–phonon polarons. The magnon–phonon coupling, always present in systems with sizeable magneto-elastic constants, is boosted if frequency and wavevector degeneracy is reached, i.e., when the quasi-particle dispersion relations intersect; this is typically the case for magnons and phonons in the gigahertz and sub-micron range.

Artificial crystals offer attractive possibilities for engineering hybrid magneto-acoustic excitations.[7,9,10] Systems gathering an artificial periodicity for both the magnonic and phononic subsystems are sometimes dubbed magnonic–phononic crystals (MPCs).[11] In these systems, by shaping the geometry, material, and anisotropy of the periodic constituents, it is possible to obtain enhanced sensitivity to the environment, chiral or unidirectional propagation,[12] or again to investigate under appropriate conditions strong coupling and dissipative coupling,[8] opening perspectives for efficient sensors and transductors. Overall, the periodic modulation of magnetostatic and elastic properties shapes the magnon and phonon band structure, respectively, as well as the wavefunctions, making MPCs ideal platforms for advancing the understanding of magneto-elastic coupling and related applications.[13]

© Author(s) 2025

Here, we report on magnonic and phononic excitations in MPCs. Via time-resolved optical magnetometry, we impulsively excite magnons and phonons, and we track the ensuing dynamics as a function of external magnetic field and time. We show that by engineering the periodicity and filling ratio of the MPC, the magnon–phonon polaron can be tuned in both frequency and magnetic field. Moreover, as we reported elsewhere,[8] the employed time-resolved approach enables the quantification of the coupling even when the condition of strong coupling is not met, i.e., when, in frequency domain, the avoided crossing collapses within the mode linewidth. We discuss here how specific features appear in frequency domain for impulsively excited magnon–phonon polarons, and how they can be due to balance of moderate coupling strength and dynamical phase of the involved modes.

We investigate one-dimensional MPCs in the form of bilayered thin ferromagnetic nanostripes (NSs) consisting of a Fe layer deposited in direct contact on a Permalloy (Py, $Ni_{80}Fe_{20}$) layer. The samples were fabricated by deep ultraviolet lithography and liftoff process;[14] with this technique, highly ordered arrays of NSs can be fabricated over a large area [Figs. 1(a) and 1(b)]. Two samples are investigated, dubbed A and B. The layer thickness is $t_{Fe} = 10$ nm and $t_{Py} = 10$ nm; for both samples, the NSs are deposited on Si (0 0 1), with the NS long axis aligned along the [100] substrate direction. The NSs have rectangular cross section [see Figs. 1(a) and 1(b)], with width $w_A = 340$ nm and $w_B = 310$ nm; for both samples, the NSs extend in length for $l = 4$ mm. The inter-NS spacing is $d_A = 70$ nm and $d_B = 300$ nm; the overall real-space periodicity is $D_A = 410$ nm and $D_B = 610$ nm. Thus, the main difference between the two samples is the NS separation and the resulting filling ratio ($r_A = 0.83$ and $r_B = 0.51$). Note that, to first order, a bilayered NS can be modeled as composed of an effective ferromagnetic material with properties corresponding to the volume average of the layer materials.[15]

Via dipolar magnetic interaction, the NSs form a magnonic crystal, with tailored magnon bands for in-plane propagation; moreover, the NSs periodically load the substrate altering its boundary conditions at the surface, resulting in modulation of the surface acoustic properties, making the sample a surface phononic crystal. The correspondence between the acoustic and magnetic periodicity results in efficient hybridization between the two excitations, as the wavevector matching is always met. The magnonic band structure for these samples was previously measured in the magnetostatic surface-wave configuration by Brillouin Light Scattering (BLS).[15] Analogous reciprocal-space periodicity is reported for the surface-phonon bands in similar samples.[11,16]

Hybrid magnon–phonon dynamics was investigated via time-resolved Magneto-Optical Kerr Effect (tr-MOKE) employing near infrared (NIR) pump ($\lambda_{pump} = 1028$ nm) and visible probe pulses ($\lambda_{probe} = 514$ nm). The optical end-station is sketched in Fig. 1(c); further details are reported in the supplementary material and are published elsewhere.[17] The sample lies in the vertical (x, y) plane. The external magnetic field B_{ext} is applied in-plane (IP). The azimuthal angle φ between B_{ext} and the NS long axis, which is also the magnetic easy axis (EA) of the sample, can be varied in the full 2π range: $\varphi = 0°$ corresponds to $B_{ext} \parallel$ EA, $\varphi = 90°$ corresponds to $B_{ext} \perp$ EA.

In the adopted tr-MOKE scheme, the NIR pump pulse is mostly absorbed by the metallic NSs. The resulting spatially periodic heating of the sample impulsively excites phonons and magnons compatible with their band structure and the spatial distribution of deposited energy. Details on the excitation mechanisms are reported in the supplementary material. This approach has close similarity with Transient Grating spectroscopy, which indeed is routinely employed to probe phonon dispersion and heat diffusion,[18] and has been recently used for excitation of coherent magnons.[19] From the tr-MOKE experiment we obtain time-domain maps where the recorded intensity oscillates in time as due to the magnonic and phononic dynamics; in Fig. 2, we report the Fast Fourier Transform (FFT) magnitude of such maps, as a function of frequency and B_{ext} strength; we refer to the supplementary material for exemplary time-domain maps. The results are reported for four values of φ. The spectral resolution of the FFT maps is given by the total observation window of 3.3 ns in time domain, resulting in a frequency-domain resolution no better than 600 MHz in FWHM.

In each map, two horizontal bands are observed: such field-independent flat modes are associated to phonons excited by the impulsive inhomogeneous heating of the sample. As reported in the literature,[7,20] the lower mode is a pseudo-Rayleigh wave, while the higher mode is mostly a localized width-breathing of the NSs. Consistently,

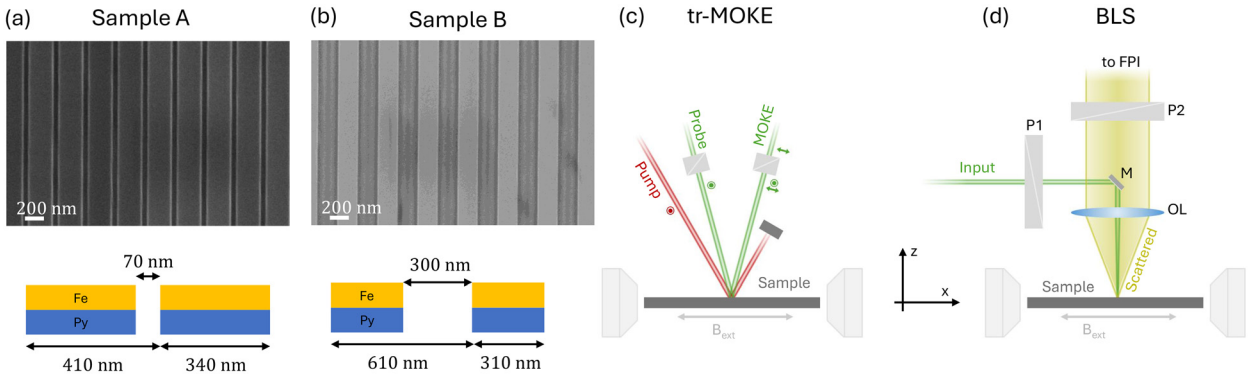

FIG. 1. (a) and (b) Top: SEM images of the surface of sample A (a) and sample B (b). Bottom: cross-sectional sketch of the samples (not to scale). (c) Sketch of the tr-MOKE end-station. Pump and probe pulses are *s*-polarized and impinge on the sample surface at small angles from the surface normal (<12°). The reflected beam exhibits a MOKE-rotated polarization, which is selected via a polarizer on the detection branch. The sample lies in the vertical (x, y) plane between the poles of an electromagnet producing a static magnetic field B_{ext}. (d) Sketch of the BLS setup. The input beam is polarized via the polarizer P1, reflected by the mirror M, and focused normal to the sample surface via the objective lens OL. The scattered light within a finite solid angle is collected by OL, analyzed in polarization via the polarizer P2, and sent to a Fabry–Pérot interferometer (FPI). For both tr-MOKE and BLS, the sample can rotate around the *z* axis, with tunable azimuthal angle φ.

22 July 2025 09:02:09

© Author(s) 2025

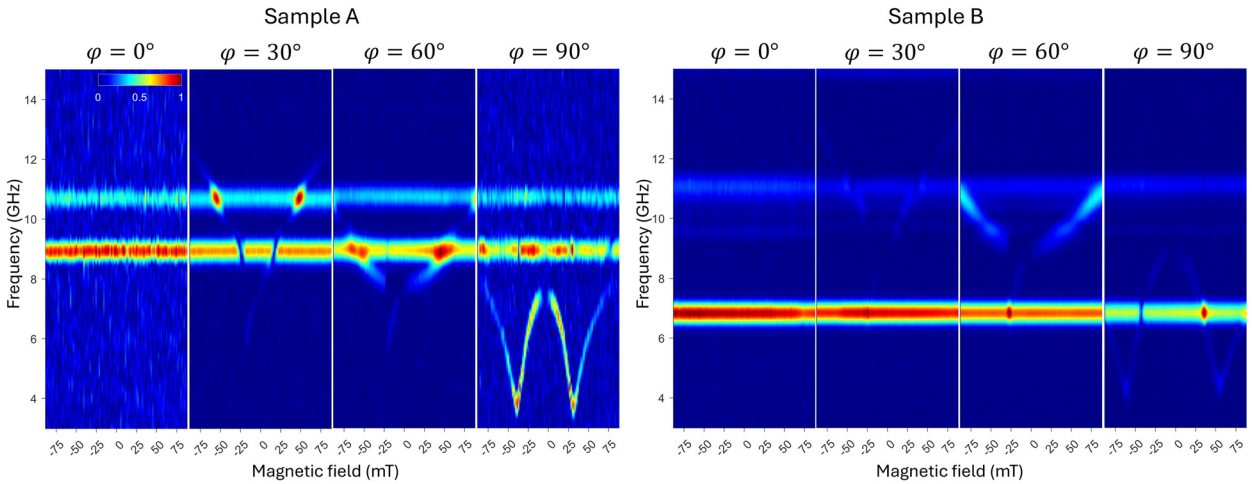

FIG. 2. Maps of the FFT magnitude computed from the time-domain tr-MOKE traces for sample A (left) and sample B (right) at four values of φ. In all maps, B_{ext} is swept from positive to negative values; each map is normalized to its maximum. Two flat non-dispersive modes are observed, at frequency approximately 8.9 and 10.7 GHz for sample A, and 6.8 and 11.1 GHz for sample B; such modes are associated with phonons. For $\varphi > 0°$ also a dispersive mode is observed, associated with a magnon.

sample B exhibits lower Rayleigh-wave frequency and higher breathing-mode frequency, as due to the longer periodicity and slightly narrower NS width. The frequency of such acoustic modes scales almost linearly with the geometrical parameters of the samples: for the Rayleigh wave, the frequency scales with the overall MPC periodicity ($D_A/D_B \approx 0.7$), while for the breathing mode it scales with the NS width ($w_B/w_A \approx 0.9$).

The maps in Fig. 2 also display non-flat modes associated with the uniform magnetization precession in the MPCs. Generation of magnetization precessional motion (namely, magnons) via pulsed laser pumping is largely reported in the literature for similar systems.[7,21] We further confirmed such assignment via BLS and micromagnetic simulations.

Spectra from thermally excited magnons were measured via BLS;[22] a sketch of the experimental setup is presented in Fig. 1(d). The spectra were recorded in air, at room temperature, in the backscattering configuration employing visible probe laser ($\lambda_{BLS} = 532$ nm) at normal incidence. Micromagnetic simulations were conducted using mumax[3]. We refer the readers to the supplementary material for further details.

In Fig. 3, we report comparison of the magnon field-dependence obtained from tr-MOKE, BLS, and micromagnetic simulations. In general, good agreement is obtained, confirming the assignment to the uniform magnon precession. For both samples, the magnon band redshifts in frequency for larger φ: this results from the increasing contribution of demagnetizing fields to the overall free energy when $B_{ext} \perp$ EA. The same phenomenology is reported in the literature.[20] Moreover, the magnon bands are quite similar in the two samples for $\varphi \leq 60°$, while a major discrepancy arises at $\varphi = 90°$, especially in the field position of the frequency minima. This is consistent with the fact

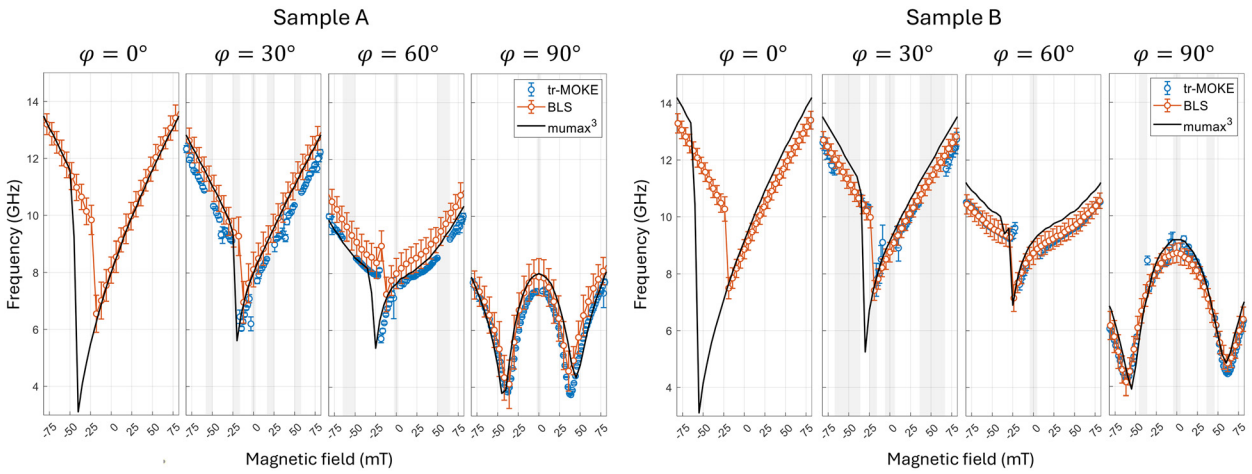

FIG. 3. Comparison of the magnon mode dispersion obtained via tr-MOKE (blue circles), BLS (orange circles), and micromagnetic simulations (black line). The vertical shaded bars highlight regions where extraction of magnon frequency from tr-MOKE data was not possible due to crossing to a phonon mode or to zero amplitude.

22 July 2025 09:02:09

© Author(s) 2025

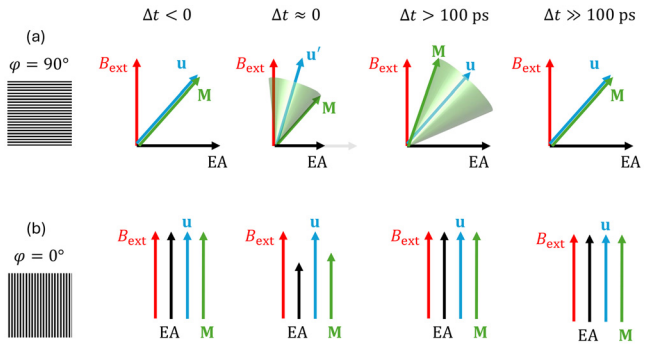

FIG. 4. Sketch of the effect of the pump on magnetization and shape anisotropy at four pump–probe delays. For non-collinear B_{ext} and EA [$\varphi = 90°$, panel (a)], the rotation of the equilibrium axis from $\mathbf{u}$ to $\mathbf{u}'$ determines coherent magnetization precession. For $B_{ext} \parallel$ EA [$\varphi = 0°$, panel (b)], only magnetization quenching and recovery are observed.

that the NS cross section is similar in the two samples, the major difference being the filling ratio and periodicity. Indeed, when the sample magnetization has a large projection along EA, its dynamics is mostly determined by the NS geometry and aspect ratios; in contrast, for $B_{ext} \perp$ EA strong demagnetizing fields arise from the edge of each NS and their influence on the magnetization dynamics strongly depends on the inter-NS distance. A major discrepancy between experiments and simulations is observed for $\varphi = 0°$ and 30° in the field position for the frequency minima; this is related to the coercivity of the NS array, which depends on several factors, including the size distribution of the NSs, defects, edge roughness, and finite temperature. None of these aspects are accounted for in the simulation.

From Figs. 2 and 3, we see that in tr-MOKE measurements the magnon mode is not observed (i.e., displays zero spectral weight) for weak B_{ext} at any φ, and for $\varphi = 0°$ at any B_{ext}. As reported in the literature, pump-induced coherent magnetization precession results from impulsive heating and reduction of the magnetization anisotropy.[21] Referring to Fig. 4, two different scenarios are identified. For $\varphi = 90°$ [panel (a)], at $\Delta t < 0$ the magnetization $\mathbf{M}$ is directed along an equilibrium axis $\mathbf{u}$, which is determined by the vectorial sum of B_{ext} and the shape anisotropy field; in this case, the anisotropy field is directed along EA, so $\mathbf{u}$ lies IP at an intermediate angle between B_{ext} and EA. When the sample is heated by the pump ($\Delta t = 0$), the anisotropy field changes in strength, and the new equilibrium axis $\mathbf{u}'$ lies at a different azimuth; $\mathbf{M}$ starts to precess about $\mathbf{u}'$. After heat transport sets in [in ferromagnetic metals typically after about 10 ps (Ref. 21)], the equilibrium axis goes back to $\mathbf{u}$; however, $\mathbf{M}$ is out of equilibrium and keeps precessing, now about $\mathbf{u}$, in a free induction decay fashion until its natural damping. For $\varphi = 0°$ [panel (b)], for $\Delta t < 0$ B_{ext}, EA and $\mathbf{u}$ are collinear. In this scenario, the reduction of anisotropy field induced by the pump does not set a different direction for the equilibrium axis, so the only effect observed is magnetization quenching and recovering. Thus, only in the first scenario the pump induces coherent magnetization precession, justifying the absence of the coherent magnon mode from the tr-MOKE data for $\varphi = 0°$. Similarly, for vanishing B_{ext} no coherent precession is triggered, as $\mathbf{M}$ remains parallel to the equilibrium anisotropy axis at any time delay.

We now discuss the features observed via tr-MOKE at the magnon–phonon crossing points. Referring to the signal intensity in Fig. 2, the most evident feature is that the spectral weight can display enhancement or depletion, depending on the experimental configuration. This cannot be immediately interpreted as a variation of the coupling strength as a function of φ, nor as a dependence on the strain components involved; even the modification of coherent into dissipative magnon–phonon coupling cannot be assumed as a straightforward explanation.

Focusing on sample B for $\varphi = 90°$, we report in Fig. 5 the FFT magnitude together with the spectral phase; as highlighted by the ellipses [panel (a)], the spectral weight of the FFT magnitude is either enhanced or depleted depending on the field being positive or negative, respectively. Looking at the spectral phase [panel (b)], the only difference between the two crossings is the magnon mode swapping the dynamical phase by π upon passing beyond the axis $B_{ext} = 0$ mT. We conclude that the enhancement/depletion feature is a *coarse structure*

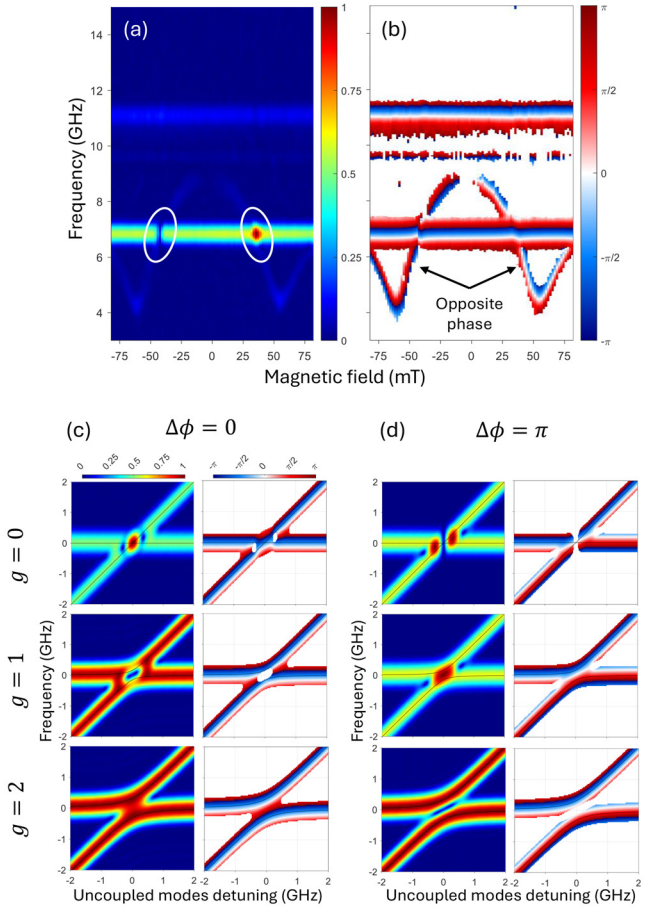

FIG. 5. FFT magnitude (a) and spectral phase (b) of tr-MOKE for sample B at $\varphi = 90°$. The white ellipses in (a) highlight the different behavior (enhancement or depletion of the spectral weight) at the magnon–phonon crossing; the spectral phase in panel (b) shows a π-flip of the magnon dynamical phase. (c) and (d) Numerical simulations of FFT magnitude and spectral phase for coherent coupling of two modes in the proximity of degeneracy, for three values of coupling strength g. In panel (c), the modes are assumed with the same dynamical phase ($\Delta\phi = 0$); opposite dynamical phase ($\Delta\phi = \pi$) is assumed in panel (d). The computed frequency for the coupled modes is reported as black solid lines.

22 July 2025 09:02:09

© Author(s) 2025

in the mode crossing, which mainly relates to the dynamical phases of the interacting modes.

To substantiate this picture, following the literature,[23] we performed systematic computations of the spectra for two quasi-degenerate modes, as a function of their frequency detuning. The spectra are computed as FFT of simulated time-domain maps, in analogy to the experimental data acquired via tr-MOKE; details are reported in the supplementary material. Three values for the coupling strength g and two values for the relative dynamical phase $\Delta\phi$ were considered. The two-dimensional maps for the calculated FFT magnitude and spectral phase are reported in Figs. 5(c) and 5(d); the calculated theoretical eigenvalues are shown as black solid lines in each panel. In order to allow a direct comparison to the experimental data, the simulated time-window was fixed to 3 ns, resulting in smearing of the FFT peaks along the frequency axis by about 600 MHz in FWHM; the intrinsic damping of the modes was assumed negligible in order to highlight the merely instrumental contribution.

For $g = 0$ rad/ns (no coupling), the FFT magnitude at the crossing strongly depends on the relative phase of the modes: coherent superposition of independent modes with same or opposite dynamical phase results in enhancement or depletion of the spectral weight, respectively. For $g = 1$ rad/ns (weak coupling), the modes start to hybridize and experience frequency repulsion (see the black solid lines), but the frequency gap is smaller than the spectral resolution. Partial spectral superposition determines again enhancement and depletion in the spectral weight, depending on the relative phase. For $g = 2$ rad/ns (strong coupling), the two hybridized branches are well separated and no artifact appears in the FFT magnitude. Thus, inspection of only the magnitude does not allow to disentangle coupling and dynamical phase effects in the case of zero and weak coupling. Combined analysis of the spectral phase could help in this job.

The results we reported show that one-dimensional MPCs exhibit tunability in the magnonic and phononic excitations. Even relying on simple NS geometry (regular spacing and rectangular cross section), the phononic modes can be shifted in the few-gigahertz range changing their aspect ratio, periodicity, and filling ratio (see the flatband modes in Fig. 2). The magnonic mode displays strong dependence on B_{ext} as well as on φ. This allows to envision tunable magnonic–phononic devices, where employing advanced lithographic processes (e-beam or transient grating-based[24]) it could be possible to push the dynamics toward the 100-GHz regime, possibly in addition to antiferromagnets with high-frequency magnonic precession.

Moreover, via the optical time-resolved approach, we highlighted crossing of magnon and phonon modes, a condition in which the excitations potentially display efficient hybridization. We evidenced how for poorly resolved FFT, i.e., when the spectral resolution is coarser or comparable to the frequency separation of the coupled modes, the magnitude can display features not related to the physics driving the mode coupling, but only due to trivial dynamical phase effects. The spectral phase, on the other hand, seems more reliable in the assessment of the coupling: proper modeling of the spectral phase dependence could be a viable road for the investigation of weakly coupled systems. We conclude highlighting that the frequency-domain features are a result of the time-resolved approach we employ. The impulsive excitation generates a phase-coherent population of the hybridizing magnon and phonon modes. Quantitative comparison to frequency-domain techniques leveraging incoherent (e.g., thermally activated) modes could be relevant in understanding the role played by coherence in the hybridization process.

See the supplementary material for details on the experimental methods, computational methods, and data analysis.

This work is performed in the framework of the Nanoscience Foundry and Fine Analysis (NFFA-MUR Italy Progetti Internazionali) facility. R.C. acknowledges the support of the Italian Ministry of Foreign Affairs and International Cooperation (MAECI), under Grant No. PGR12320—U-DYNAMEC—CUP B53C23006060001. G.G., G.P., and R.S. acknowledge the support of the European Union–NextGenerationEU, Mission 4, Component 1, under the Italian Ministry of University and Research (MUR) National Innovation Ecosystem Grant Nos. ECS00000041-VITALITY-CUP B43C22000470005 and J97G22000170005. GG also acknowledges funding from the EU project MandMEMS, Grant No. 101070536. GP acknowledges support from PNRRMUR project PE0000023-NQSTI. A.O.A. and G.G. acknowledge the funding received from the Royal Society through the Wolfson Fellowship and International Exchanges IEC\R2\222074.

AUTHOR DECLARATIONS

Conflict of Interest

The authors have no conflicts to disclose.

Author Contributions

P. Carrara: Conceptualization (equal); Data curation (equal); Formal analysis (equal); Investigation (equal); Writing – original draft (lead); Writing – review & editing (equal). **M. Brioschi:** Conceptualization (equal); Data curation (equal); Formal analysis (equal); Investigation (equal); Writing – review & editing (equal). **R. Silvani:** Data curation (equal); Investigation (equal); Writing – review & editing (equal). **A. O. Adeyeye:** Funding acquisition (equal); Investigation (equal); Supervision (equal); Writing – review & editing (equal). **G. Panaccione:** Conceptualization (equal); Funding acquisition (equal); Supervision (equal); Writing – review & editing (equal). **G. Gubbiotti:** Data curation (equal); Funding acquisition (equal); Investigation (equal); Supervision (equal); Writing – review & editing (equal). **G. Rossi:** Funding acquisition (equal); Supervision (equal); Writing – review & editing (equal). **R. Cucini:** Conceptualization (equal); Data curation (equal); Funding acquisition (equal); Investigation (equal); Supervision (equal); Writing – review & editing (equal).

DATA AVAILABILITY

The data that support the findings of this study are openly available in Zenodo at http://doi.org/10.5281/zenodo.15641909, Ref. 25.

REFERENCES

[1]A. V. Chumak, V. I. Vasyuchka, A. A. Serga, and B. Hillebrands, "Magnon spintronics," Nat. Phys. **11**, 453–461 (2015).
[2]A. Barman, G. Gubbiotti, S. Ladak, A. O. Adeyeye, M. Krawczyk, J. Gräfe, C. Adelmann, S. Cotofana, A. Naeemi, V. I. Vasyuchka *et al.*, "The 2021 magnonics roadmap," J. Phys.: Condens. Matter **33**, 413001 (2021).

22 July 2025 09:02:09

© Author(s) 2025

[3]A. V. Chumak, P. Kabos, M. Wu, C. Abert, C. Adelmann, A. O. Adeyeye, J. Åkerman, F. G. Aliev, A. Anane, A. Awad *et al.*, "Advances in magnetics roadmap on spin-wave computing," IEEE Trans. Magn. **58**, 1–72 (2022).
[4]D. Lachance-Quirion, Y. Tabuchi, A. Gloppe, K. Usami, and Y. Nakamura, "Hybrid quantum systems based on magnonics," Appl. Phys. Express **12**, 070101 (2019).
[5]J. Janušonis, T. Jansma, C. Chang, Q. Liu, A. Gatilova, A. Lomonosov, V. Shalagatskyi, T. Pezeril, V. Temnov, and R. Tobey, "Transient grating spectroscopy in magnetic thin films: Simultaneous detection of elastic and magnetic dynamics," Sci. Rep. **6**, 29143 (2016).
[6]P. Carrara, M. Brioschi, E. Longo, D. Dagur, V. Polewczyk, G. Vinai, R. Mantovan, M. Fanciulli, G. Rossi, G. Panaccione *et al.*, "All-optical generation and time-resolved polarimetry of magnetoacoustic resonances via transient grating spectroscopy," Phys. Rev. Appl. **18**, 044009 (2022).
[7]F. Godejohann, A. V. Scherbakov, S. M. Kukhtaruk, A. N. Poddubny, D. D. Yaremkevich, M. Wang, A. Nadzeyka, D. R. Yakovlev, A. W. Rushforth, A. V. Akimov *et al.*, "Magnon polaron formed by selectively coupled coherent magnon and phonon modes of a surface patterned ferromagnet," Phys. Rev. B **102**, 144438 (2020).
[8]P. Carrara, M. Brioschi, R. Silvani, A. Adeyeye, G. Panaccione, G. Gubbiotti, G. Rossi, and R. Cucini, "Coherent and dissipative coupling in a magnetomechanical system," Phys. Rev. Lett. **132**, 216701 (2024).
[9]A. Chumak, A. Serga, and B. Hillebrands, "Magnonic crystals for data processing," J. Phys. D **50**, 244001 (2017).
[10]D. Hatanaka, M. Asano, H. Okamoto, and H. Yamaguchi, "Phononic crystal cavity magnomechanics," Phys. Rev. Appl. **19**, 054071 (2023).
[11]V. Zhang, F. Ma, H. Pan, C. Lin, H. Lim, S. Ng, M. Kuok, S. Jain, and A. Adeyeye, "Observation of dual magnonic and phononic bandgaps in bicomponent nanostructured crystals," Appl. Phys. Lett. **100**, 163118 (2012).
[12]L. Liao, J. Puebla, K. Yamamoto, J. Kim, S. Maekawa, Y. Hwang, Y. Ba, and Y. Otani, "Valley-selective phonon-magnon scattering in magnetoelastic superlattices," Phys. Rev. Lett. **131**, 176701 (2023).
[13]L. Liao, J. Liu, J. Puebla, Q. Shao, and Y. Otani, "Hybrid magnon-phonon crystals," npj Spintronics **2**, 47 (2024).
[14]A. Adeyeye and N. Singh, "Large area patterned magnetic nanostructures," J. Phys. D **41**, 153001 (2008).
[15]R. Silvani, M. Kostylev, A. O. Adeyeye, and G. Gubbiotti, "Spin wave filtering and guiding in permalloy/iron nanowires," J. Magn. Magn. Mater. **450**, 51–59 (2018).
[16]H. Pan, V. L. Zhang, K. Di, M. H. Kuok, H. S. Lim, S. C. Ng, N. Singh, and A. O. Adeyeye, "Phononic and magnonic dispersions of surface waves on a permalloy/barc nanostructured array," Nanoscale Res. Lett. **8**, 115 (2013).
[17]M. Brioschi, P. Carrara, V. Polewczyk, D. Dagur, G. Vinai, P. Parisse, S. Dal Zilio, G. Panaccione, G. Rossi, and R. Cucini, "Multidetection scheme for transient-grating-based spectroscopy," Opt. Lett. **48**, 167–170 (2023).
[18]U. Choudhry, T. Kim, M. Adams, J. Ranasinghe, R. Yang, and B. Liao, "Characterizing microscale energy transport in materials with transient grating spectroscopy," J. Appl. Phys. **130**, 231101 (2021).
[19]P. R. Miedaner, N. Berndt, J. Deschamps, S. Urazhdin, N. Khatu, D. Fainozzi, M. Brioschi, P. Carrara, R. Cucini, G. Rossi *et al.*, "Excitation and detection of coherent nanoscale spin waves via extreme ultraviolet transient gratings," Sci. Adv. **10**, eadp6015 (2024).
[20]C. L. Chang, R. R. Tamming, T. J. Broomhall, J. Janusonis, P. W. Fry, R. I. Tobey, and T. J. Hayward, "Selective excitation of localized spin-wave modes by optically pumped surface acoustic waves," Phys. Rev. Appl. **10**, 034068 (2018).
[21]M. Van Kampen, C. Jozsa, J. Kohlhepp, P. LeClair, L. Lagae, W. De Jonge, and B. Koopmans, "All-optical probe of coherent spin waves," Phys. Rev. Lett. **88**, 227201 (2002).
[22]G. Carlotti and G. Gubbiotti, "Magnetic properties of layered nanostructures studied by means of Brillouin light scattering and the surface magneto-optical Kerr effect," J. Phys.: Condens. Matter **14**, 8199 (2002).
[23]M. Harder, B. Yao, Y. Gui, and C.-M. Hu, "Coherent and dissipative cavity magnonics," J. Appl. Phys. **129**, 201101 (2021).
[24]F. Bencivenga, R. Cucini, F. Capotondi, A. Battistoni, R. Mincigrucci, E. Giangrisostomi, A. Gessini, M. Manfredda, I. Nikolov, E. Pedersoli *et al.*, "Four-wave mixing experiments with extreme ultraviolet transient gratings," Nature **520**, 205–208 (2015).
[25]P. Carrara, M. Brioschi, R. Silvani, A. O. Adeyeye, G. Panaccione, G. Gubbiotti, G. Rossi, and R. Cucini (2025). "Dataset for paper 'Field- and frequency-tunable magnon-phonon resonances in arrays of ferromagnetic nanostripes' by P. Carrara *et al.*," Zenodo. http://doi.org/10.5281/zenodo.15641909

22 July 2025 09:02:09

© Author(s) 2025